Article

Effect of Photoinitiators Doped in PDMS for Femtosecond-Laser Writing: Characterization and Outcomes

Antsar R. Hlil,* Jean-Sebastien Boisvert, Hatem M. Titi, Yalina Garcia-Puente, Wagner Correr, Sebastien Loranger, Jyothis Thomas, Ali Riaz, Younès Messaddeq, and Raman Kashyap
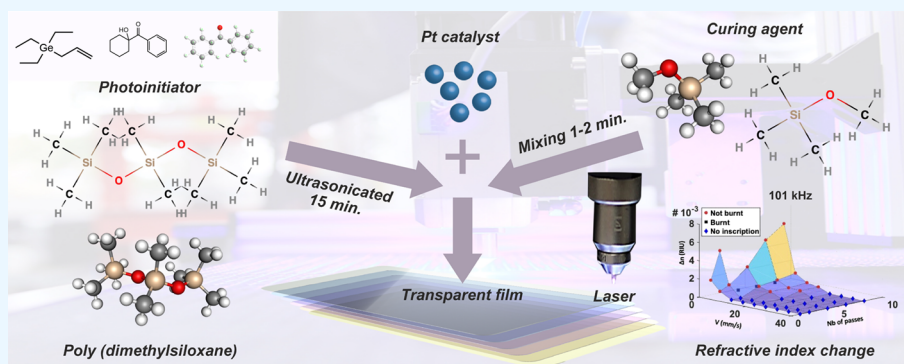
Read Online

ACCESS | ılıl Metrics & More | Article Recommendations | SI Supporting Information

ABSTRACT: Herein, we have characterized in depth the effect of femtosecond (fs)-laser writing on various polydimethylsiloxane (PDMS)-based composites. The study combines systematic and nanoscale characterizations for the PDMS blends that include various photoinitiators (organic and inorganic agents) before and after fs-laser writing. The results exhibit that the photoinitiators can dictate the mechanical properties of the PDMS, in which Young's modulus of PDMS composites has higher elasticity. The study illustrates a major improvement in refractive index change by 15 times higher in the case of PDMS/BP-Ge [benzophenone (BP) allytriethylgermane] and Irgacure 184. Additional enhancement was achieved in the optical performance levels of the PDMS composites (the PDMS composites of Irgacure 184/500, BP-Ge, and Ge-ATEG have a relative difference of less than 5% in comparison with pristine PDMS), which are on par with glasses. This insightful study can guide future investigators in choosing photoinitiators for particular applications in photonics and polymer chemistry.

1. INTRODUCTION

Lasers producing femtosecond (fs) laser pulses were first developed in the 1980s. Fs laser pulses have had a very significant impact on how we now view chemical reactions. Similarly, they have also made significant impacts in related sciences such as biochemistry, biology, and physics. Scientific curiosity keeps taking advantage of fs lasers, finding new applications, and using these tools for solving new problems.

The ultrashort pulse width and extremely high-intensity peak are some of the main exceptional characteristics. Comparing these properties to traditional laser processing, which uses longer pulse or continuous wave lasers, illustrates the advantages of fs lasers.[1,2] High precision and high quality in micro- and nanofabrication are provided by the nonthermal processes as rapid energy deposition in the material takes place.[3,4] Another major advantage of fs-direct writing is the reduction in thermal effects, which is of high importance in processing biomaterials. The aforementioned advantages provide applica-

tions in many fields, from medicine to biology,[5,6] and in the technologies of information systems and telecommunications.[7]

Performed in the absence of chemical solvents and in an ambient atmosphere, this method offers advantages in the coating, painting, and surface protection industries and has recently gained priority in these fields as an environmentally friendly material.

The refractive index is among the properties most susceptible to be modified under the fs pulse, and this modification is essential for waveguide fabrication, gratings, and couplers.[1,8−10] The versatility of fs-laser writing was well demonstrated from studies on the optical breakdown of the dielectric material to the inscription of photonic structures
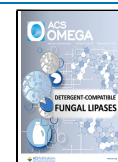
such as waveguides, Bragg gratings, and diffractive optic elements.[11−13] Fs lasers were used to write directly onto different materials, especially polymers,[14−16] including poly-methyl methacrylate (PMMA)−polystyrene (PS), poly(vinyl alcohol) (PVA), and poly(dimethylsiloxane) (PDMS). There is increasing interest in the study of PDMS for several engineering applications.[17]

PDMS is one of the widely used silicone elastomers for a variety of microfluidic devices, including lab-on-a-chip (LOC) applications.[18] It offers many advantages, including good flexibility, transparency, low cost, chemical inertness, ease of material fabrication, and high chemical and thermal stability. PDMS is also considered an emerging material for laser writing.[14] Owing to its stretchability, PDMS is a platform that has recently gained interest in the field of fs writing for the waveguide.[15] Laser processing of PDMS has also been previously reported by some researchers[19] who used a Ti:sapphire fs-pulse laser for direct patterning of PDMS stamps for microcontact printing, but there were certain limitations on serial processing and the usage of specialized lasers and positioning equipment. Various surface modifica-tions of PDMS were achieved using a CO_2-pulsed laser.[10]

The researchers observed that laser treatment induced chain ordering and porosity onto the PDMS surface, which resulted in a super-hydrophobic surface using a 248-nm KrF laser and a 266-nm laser. Other researchers introduced UV photo-sensitivity in PDMS using ultraviolet (UV) radiation, causing a bleaching reaction that severely degrades the material properties.[20] Our approach is to obtain highly tunable integrated optical devices by enhancing the fs photoinscription response of the material without damaging the material properties. It has been demonstrated that PDMS can be laser-structured using direct writing with appropriate photo-initiators[21,22] and thermoinitiators.[23] However, to the best of our knowledge, the reported literature is focused only on the surface of the materials and did not meet so far.[21,22]

Recently, we reported the photosensitization of PDMS to enhance the fs photoinscription response of the material without significantly damaging the mechanical properties, which is the key to obtaining highly tunable integrated optical devices.[24] Enhanced photosensitivity was also reported by Panusa et al.[25] using phenylacetylene as a photosensitizing agent. This procedure requires several steps that have time-dependency on the sample size and the chemical agent. Furthermore, the induction of Nd:YAG lasers for structuring PDMS has been reported by Graubner et al.[26] The authors analyzed ablation products and brought out pronounced incubation behavior. Further analysis revealed increased surface roughness following the local chemical transformation of the PDMS surface. These studies concentrated exclusively on the surface area of PDMS and noted a weakness in the surface roughness. Although many studies describing laser-irradiated polymers have been published, a clean ablation process and mechanism are yet to be achieved, as important changes in undoped PDMS continue to be reported post-irradiation.[10,19,26]

Despite the abundant literature reports, no comments on the mechanical properties of fs-exposed PDMS or the origin of the refractive index change have been presented, which raises questions about the integrity of the material after inscription. In this article, following and unlike our previous study that presented the effect organo and organometallic initiators on writing,[27] here we report in detail the properties of our

materials before and after writing. This allows controlled functionalization and homogenized concentrations of photo-sensitive polymer composites.

There are numerous underexplored and unexplored areas that are related to photosensitive PDMS. To the best of our knowledge, no full characterization of the photosensitized PDMS composite and its application for fs-laser writing have been previously reported. However, this study fully concen-trates on the optical, thermal, and structural characteristics of the photosensitized PDMS composite. The main challenge in this research is to acquire a transparent material that is suitable for fs-laser writing. Previously, we reported the fabrication of highly transparent composites of PDMS that have been evaluated through careful selection of the concentration ratio of the photosensitizer to PDMS and the choice of suitable solvents to acquire suitable conditions for fabrication.[28]

The characteristics of these materials are measured by Raman spectroscopy, thermogravimetric analysis (TGA), differential scanning calorimetry (DSC), UV−vis spectroscopy, powder X-ray diffraction (PXRD), Fourier transform infrared spectroscopy, and scanning electron microscopy (SEM). We also performed mechanical studies, namely, tensile tests immediately before and after fs-laser writing. Furthermore, a systematic study was performed on temperature-dependent structural investigation of PDMS composites using Raman spectroscopy, mechanical analysis (DMA), refractive index change (RI change), and aging. The results of this research show a significant enhancement in the RI change over our initial trials in previous studies[14] by allowing PDMS to reach optical performance levels, similar to glass. This study presents an in-depth interpretation of characteristics, and a systematic comprehensive study is needed to acquire the desired properties for potential LOC-based applications.

2. RESULTS AND DISCUSSION

2.1. UV−Vis (Transmittance or Absorbance) Charac-terization. The transparency of the composites, as well as unmodified PDMS and their optical transmission properties, was assessed by UV−vis measurements as a means to determine their potential fs writing performance (Figure 1).
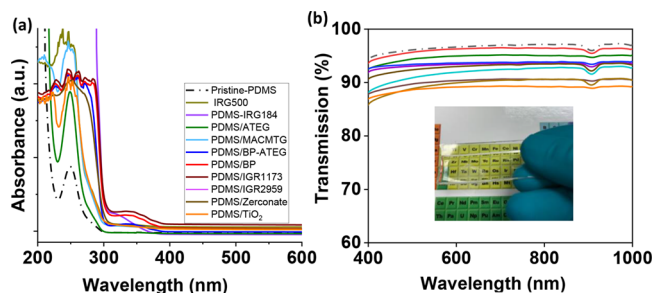

Figure 1. (a) UV−vis absorption spectra of the polymer composites incorporating different photoinitiators. (b) In the visible range for a transmittance spectrum of PDMS and PDMS blends. Note that all the measured samples consist of 1 mm thickness.

Transparent polymers, such as PDMS, are often used in combination with fs lasers because they allow for deep penetration of the laser beam into the material. This is important because fs lasers have very short pulse durations, on the order of femtoseconds or attoseconds, and are capable of delivering very high energy densities. To take advantage of

these properties, the laser beam needs to be able to penetrate deep into the material, which is facilitated by the transparency of the polymer. Transparent polymers also allow for non-destructive imaging of the material during and after the laser treatment. This is useful for monitoring and characterizing the structures formed on the surface of the polymer. Additionally, since fs lasers also emit a large amount of heat, the transparent polymer also helps to minimize heat-induced damage by dissipating the heat quickly.[29,30]

In Figure 1a, the absorption peaks in the range of 240−276 nm correspond to the formation of ketones and radicals by the photosensitizer. All UV−vis behaviors of the polymer composites demonstrate the incorporation of the different photoinitiators and are described in further detail (see Supporting Information, for more details Figure S1). These effects clearly suggest that the presence of the photoinitiator in PDMS blends explains the changes in the transmission. In addition, Figure 1b shows that the UV−vis transmission spectra of the 1-mm-thick films are relatively unaffected in the range of visible light (400−900 nm). Minor changes in the transmission ranges between 92−95 and 86−88% are observed for organic and inorganic photoinitiators, respectively. The PDMS composites of Irgacure 184/500, BP-Ge, and Ge-ATEG have a relative difference of less than 5% in comparison with pristine PDMS. In contrast, higher differences were found for the remaining composites, as illustrated in Figure 1. These differences in transmission values can be caused by scattering and Fresnel reflection at interfaces. It is worth noting that as UV−vis spectroscopy provides only qualitative information about the PDMS structures, additional characterization was performed.

2.2. Refractive Indices. The prism coupling technique was used to determine the refractive indices[31] for five wavelengths (473, 632.8, 964, 1311, and 1552 nm) by using a Metricon model 2010/M prism coupler.[32] The detailed results are available in Supporting Information Table S1. RI measurements for polymer composites and pristine PDMS are conducted before exposure to the fs laser. The results show that with the increase in wavelength, the RI decreases slightly, from approximately 1.4273 to 1.4104, as expected for a transparent colorless material (normal dispersion) with a significant variation only at 532 and 1538 nm. For example, the highest refractive index at 532 nm is 1.4273 for the polymer composite PDMS/BP-Ge and decreases with the increase in wavelengths. As shown in Figure 2, there are no significant differences in the RI values measured at 1538 nm for all the composites except for PDMS/BP-Ge; the details are summarized in the Supporting Information.

2.3. Measurements of the Refractive Index Change. As shown in Figure 3a−e, physical characterization of the polymer was performed, and the results revealed that the highest RI change was 15 times larger than the best result obtained with pure PDMS, indicating the successful incorporation of the photoinitiator into the polymer network. A wavelength of $\lambda = 515$ nm was used to influence the course of the reaction during the writing, and this influence can be adjusted by changing the writing speed, the number of passes, and the repetition rate, as detailed in our previous report.[28] This enhancement indicates the successful incorporation of the photoinitiators into the polymer network. Detailed measurements are available in the Supporting Information.

2.4. Thermogravimetric Analysis (TGA). The thermal properties of polymer composites are important in engineering
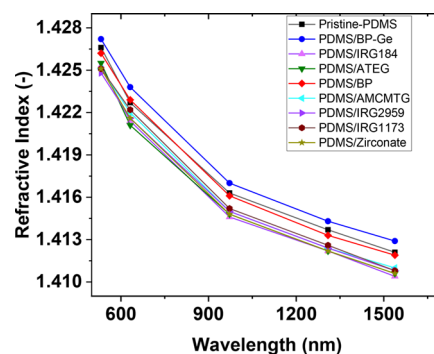

Figure 2. Refractive index vs wavelength of the studied materials before writing. A comparison between PDMS composites at five different wavelengths (473, 632.8, 964, 1311, and 1552 nm) was measured by the prism coupling method.

applications. It is essential to understand the thermal stability of our materials before exposing the films to the fs laser to avoid damaging the films. Fs-laser writing deposits a lot of energy in a small local volume, which leads to an increase in the local temperature. If the material has high thermal stability without reaching the degradation limit, it can be considered a good candidate for writing applications. Hence, the TGA of pristine and doped PDMS heated up to 800 °C using a constant heating rate of 10 °C min^{-1} were analyzed in air/nitrogen atmospheres. The decomposition was evaluated at different percentages of weight loss ($T_{d,5wt\%}$ and T_{max}) (Table 1). All the studied TGA traces of various polymer composites under a stream of nitrogen are shown in Figure S2. Note that the composites were also studied in an air atmosphere (Figure 4a) because they may have specific applications in an oxidative environment. Moreover, we would like to emphasize that the weight loss of the composites is influenced by the wt % and the type of photoinitiator agent.

As observed in Figure 4a, the decomposition weight loss of pristine and doped PDMS mostly occurred at temperatures higher than 350 °C. The results show that all composites and pristine PDMS display a high heat resistance, with only 1% weight loss between 265 and 290 °C. The initial thermal decomposition temperature ($T_{d,5wt\%}$) is defined as the temperature at which the mass loss of 5 wt % occurs, and it was observed in the range of 390−406 °C in N$_2$ or in the range of 363−391 °C when the air environment was used. The observed thermal stabilities of various composites are high and will therefore avoid degradation of the samples under fs lasers.

Notably, the degradation behavior of the composites in the air begins at lower temperatures and has multiple degradation steps, of which rapid decomposition was observed at approximately around 581−646 °C. The residual weight loss ranged between 23 and 51% in N$_2$, whereas it is observed to be 40−67% in air. This is attributed to the difference in pyrolysis characteristics of the different agents in the polymers. These differences and similarities are even more visible in the analyzed polymer DTG curves, as shown in Figure S3a,b. For the pristine Sylgard-PDMS, decomposition occurred in two steps, indicating that there is a chemical transition that can be linked to the depolymerization of the PDMS chain through the breaking of Si−O bonds.[33] However, for the doped PDMS, those steps did not occur, indicating that the material undergoes direct decomposition. However, in the presence of air, the thermal behavior of the pristine PDMS is completely different, as shown in Figure 4a. The degradation of PDMS
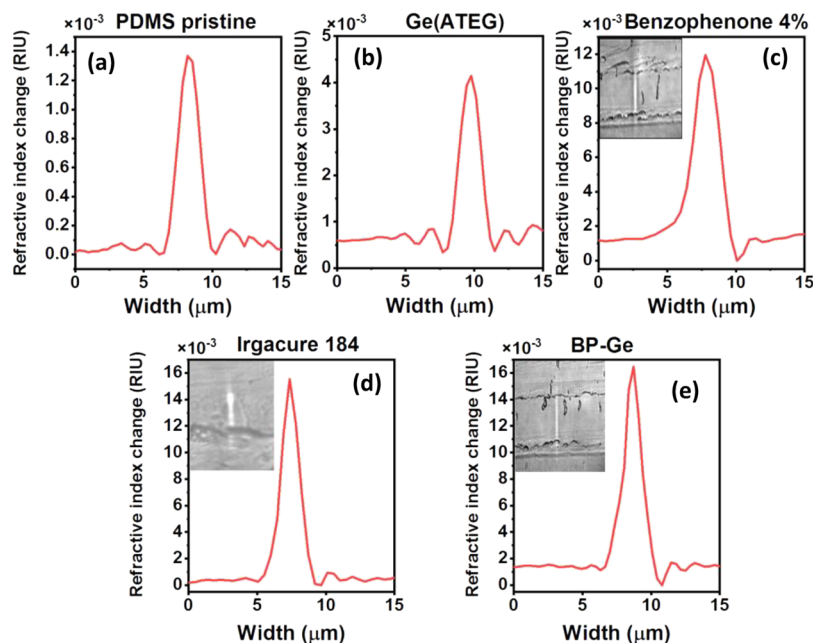
Figure 3. Fs-laser written waveguide. The corresponding refractive index profiles of (a) pristine PDMS with parameters: repetition rate 606 kHz, 8 passes, and 25 mm·s^{-1}; (b) with parameters: 101 kHz, 8 passes, and 20 mm·s^{-1}; (c) PDMS/BP with parameters: repetition rate 606 kHz, 2 passes, 5 mm·s^{-1}, and a near-field optical micrograph of the cross-section of the waveguide; (d) PDMS/Irgacure 184 with parameters: repetition rate 101 kHz, 2 passes, 5 mm·s^{-1}, and a near-field optical micrograph of the cross-section of the waveguide; and (e) PDMS/BP + Ge(ATEG) with parameters: repetition rate 606 kHz, 8 passes, 15 mm·s^{-1}, and a near-field optical micrograph of the cross-section of the waveguide.

Table 1. Summary of the TGA Results for All Blends under N$_2$ and Air and DSC of the Polymer Composites of PDMS^a

	TGA (°C)^a 5 wt %		total wt %^{b}			DSC	
polymer composite	N$_2$	air	N$_2$	air	T_{max} (°C)^c weight lost	T_g^d (°C)	ΔC_p^e J g^{-1} K^{-1}
pristine PDMS	406	383	53	67	581	−123.1	0.167
PDMS/ATEG	398	377	72	68	583	−122.5	0.170
PDMS/BP	400	362	72	65	628	−123.3	0.157
PDMS/BP-ATEG	400	375	55	50	615	−123.0	0.184
PDMS/IRG.184	391	364	71	44	596	−122.5	0.170
PDMS/IRG.500	375	355	63	47	655	−121.6	0.151
PDMS/IRG.1173	378	382	59	67	586	−122.7	0.180
PDMS/IRG2959	382	364	50	40	570	−122.8	0.180
PDMS/zirconite	399	380	39	52	646	−123.7	0.157
PDMS/TiO$_2$	393	362	36	53	586	−123.1	0.130
PDMS/(MACMTG) 2%	400	375	77	50	613	−122.7	0.135

^{a}(a, b, c, d) Obtained by TGA under a 25 mL/min stream nitrogen atmosphere with a constant heating ramp of 10 °C/ min. (c) T_{max} is extracted from the first derivative of the TGA, which gives the maximum degradation temperature. (d, e) Obtained by DSC under a helium atmosphere with a heating rate of 10 K/min.
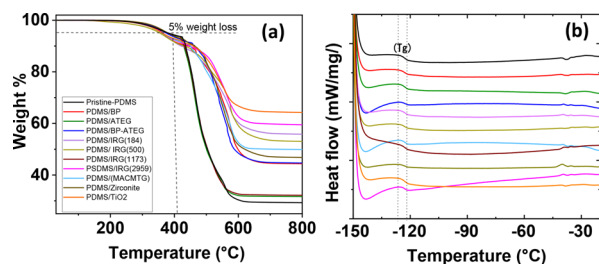

Figure 4. (a) TGA curves of the polymer composites in air. All measurements were done under a 25 mL min^{-1} stream of air, and the samples were heated up to 800 °C, at a heating rate of 10 °C min^{-1}. (b) DSC curves of the polymer composites and their corresponding T_g thermal events.

starts at lower temperatures, and more than one stage of degradation can be identified. This observation means that the pristine PDMS polymer chains were modified by crosslinking with doped agents. This result could be ascribed to the formation of the radical and oxidation of the agents and contribute to the faster initial decomposition temperature in air. It can be concluded that the initial and final temperatures of the decomposition of all samples are different. These thermal events indicate that the effect of the fs laser will vary between the different composites and should be taken into consideration during the parameter writing.

2.5. Differential Scanning Calorimetry (DSC). Figure 4b shows thermograms from the DSC measurements of the polymer composites in the presence of different photo-sensitizers. The measured glass transition temperatures (T_g) showed no significant difference in the T_g temperatures for
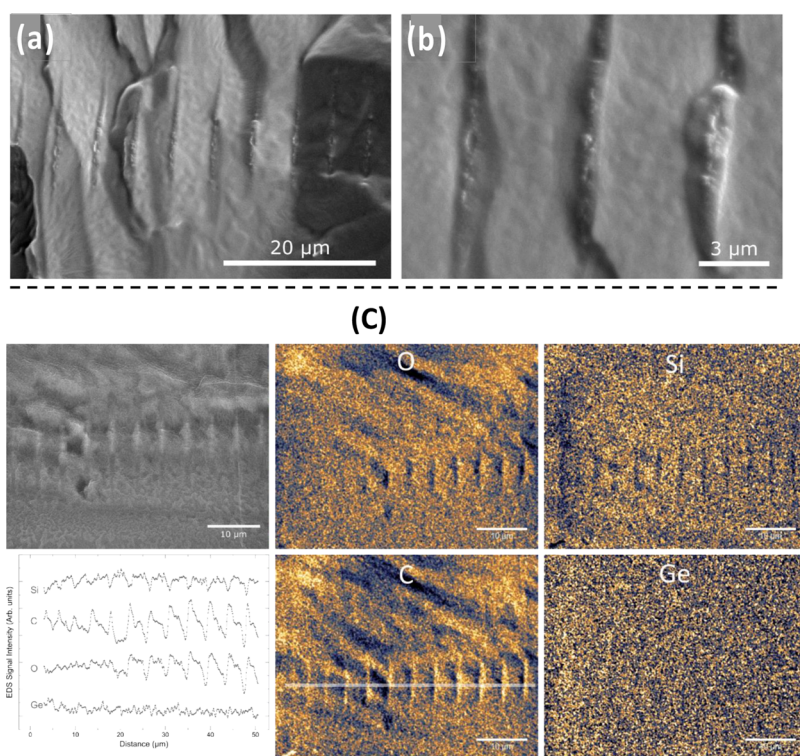
Figure 5. SEM images of (a) and (b) PDMS/BP + Ge composite cross-sections showing the laser-inscribed waveguides. (c) EDS mapping of the composite's cross-section. A higher concentration of carbon and oxygen is noticeable at the waveguides.

Sylgard-PDMS and the composites. The results indicate that the introduction of a photosensitizer does not change the glass transition temperatures. Crystallization and melting events were not clearly observed for Sylgard-PDMS, as shown in Figure 4b. The heat capacity, C_p, associated with the T_g was found to be in the range of 0.151−0.184 J g^{-1} K^{-1} with no significant changes, ΔC_p, among the polymer composites (Table 1). In the glassy state, the process requires a great degree of cooperativity between the chain segments, which is associated with a large energy barrier in the early stages of the transition. In this case, lowering the energy barrier can be achieved by increasing the temperature.

2.6. Analysis Based on Powder X-ray Diffraction (PXRD). To study the effect of the radicals on the photosensitized PDMS structure, we conducted PXRD (see the SI) before and after laser writing. The samples were studied using the EVA package (Bruker), in which the calculated crystallinity index functionality is incorporated into the software. The PDMS structure is a semi-crystalline material that has a prominent amorphous phase. To enhance the reactivity of the PDMS, the pristine samples were blended with various organic and inorganic molecules. These molecules were first tested to study whether the crystallinity of the materials was affected before exposure to writing (as fabricated). Note that all the composites were treated similarly and were thermally cured. Our goal is to find a suitable photoinitiator-based composite for *fs*-laser writing.

Initially, we studied organic molecules such as benzophenone (BP) that have a direct influence on the crystallinity of the structure (Table S2). The PDMS in this blend loses crystallinity (Figure S4); however, when switching from BP to IRG 184, amorphization was improved slightly. Other photoinitiator agents such as IRG 1173 and IRG 2959 did not improve the amorphization of the PDMS any further.

Notably, a mixture of BP and IRG 184—namely, IRG 500—also did not affect the crystallinity of the structure. Therefore, the trend in the photoinitiator agents of organic molecules on PDMS can be categorized as follows: IRG 184 > BP > IRG 1173 > IRG 500 > IRG 2959. In contrast, we have studied the influence of inorganic additives on the PDMS, and we found that using TiO_2 has a greater effect on the structure compared with ZrO_2. However, the addition of TiO_2 and ZrO_2 resulted in aggregation into the PDMS thin films, which reduces the transparency of the desired composites. Unlike TiO_2 and ZrO_2 agents, the use of a liquid agent such as the germanium complex achieves a direct reorganization of the PDMS crystallinity and preserves transparency.

As mentioned above, the original PDMS control loses crystallinity when a photoinitiator is used; however, we were interested in probing whether we could write on the film using an fs laser (515 nm), in which we found that the laser engraves the film as deep as 400 μm. In those materials, we initiated the photosynthesis by mixing the PDMS with BP, IRG 184, and/or the Ge complex; the results are organized in Table S3. The addition of 3%−4% BP (we did not exceed the addition of 4% as it results in decreased transparency of the film) results in a slight increase in amorphization owing to the reactivity of BP as a type II photoinitiator (Figure S5). The use of IRG 184, which is considered a type I photoinitiator, decreases even further the crystallinity in comparison with pristine PDMS. IRG 184 consists of two reactive radical sites on the molecule that can readily react with the PDMS functionalities. Alternatively, the blend Ge complex with IRG 184 in PDMS led to almost no change in amorphization. The reason for the low reactivity is the presence of two photoinitiators (type I) competing on the radical sites. In contrast, the addition of approximately 2% of the Ge complex, which is used as a cleaving agent, decreases the crystallinity by 7%. A pronounced
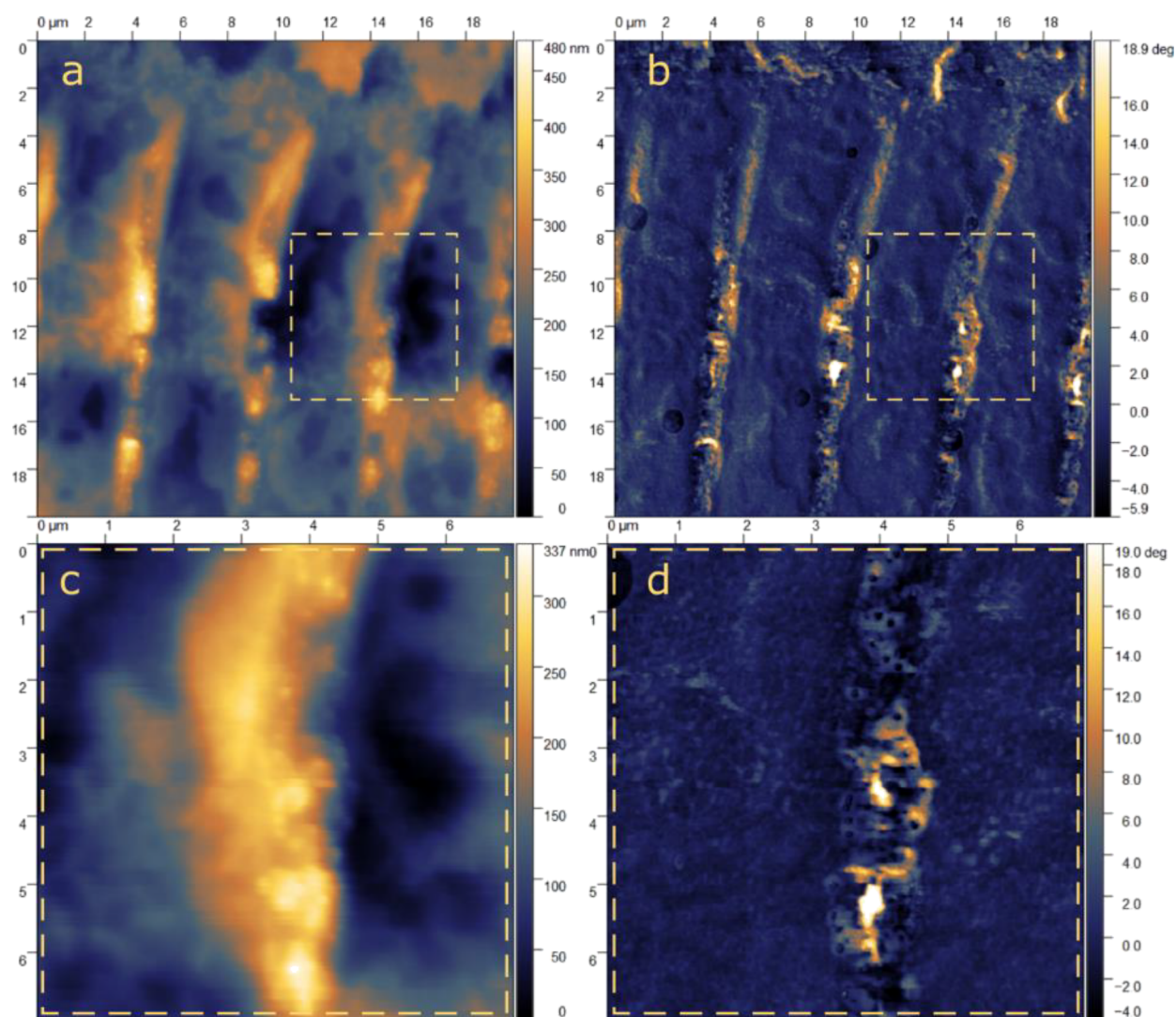
Figure 6. AFM of the PDMS/BP + Ge composite. (a) Cross-section topography created during the cryo-fracture, and (b) its respective phase image. (c) Higher magnification of the central section of a waveguide shows the presence of particles of ca. 30−40 nm. (d) Phase image of (c).

amorphization degree was obtained when the Ge agent and BP blended with PDMS. A noticeable increase in amorphization was obtained by using BP/ATEG mixed with PDMS, with an increase of 11%. The presence of both the Ge complex and BP type II photoinitiator generated competition for reacting with the PDMS radicals on the allyl functionalities and H-atoms.

2.7. Scanning Electron Microscopy (SEM) and Atomic Force Microscopy (AFM). Selected samples for SEM and atomic force microscopy (AFM) were prepared by excising the inscribed waveguides from the rest of the PDMS. The samples were then immersed in liquid nitrogen for a few minutes. Once thermalized, the samples were cryo-fractured inside liquid nitrogen. The surface of the fracture was recovered and mounted on SEM stubs using silver epoxy conductive glue. Furthermore, a Pt−Pd thin film was sputtered on the fractured surfaces to avoid excessive charging. Electron microscopy (Quanta 3D FEG, FEI) was used to image the fractured surface and identify the waveguide's relief after the fracture. In addition, X-ray energy-dispersive spectroscopy (EDS) was employed to identify and image the distribution of the elements at the cross-section.

AFM images were acquired in a Nanoscope V (Bruker) scanning probe microscope, operating in the tapping mode

with a silicon tip (Bruker), whose resonance frequency was close to 300 kHz. The mounted samples for AFM imaging required no further preparation after cross-sectioning in liquid nitrogen. The height and phase images were acquired directly from the surface of the fracture, i.e., the waveguide's cross-section. The images were processed using the Gwydion SPM analysis software.

The SEM images of the cryo-fracture of the sample PDMS/BP-Ge show the cross-section of the laser-inscribed waveguides (Figure 5a). The PDMS matrix displays a classical conchoidal fracture characteristic of glassy materials, while 10 parallel waveguides can be noticed aligned vertically. The cross-section of the waveguides has an average length of 18.0 ± 0.5 μm, an average maximum width of 1.0 ± 0.15 μm, and a periodicity value of 5.2 ± 0.2 μm. A higher magnification of the waveguide's cross-section (Figure 5b) demonstrates that the fracture of the waveguide differs from the PDMS matrix, with the waveguide having a grainy appearance.

EDS mapping allows the identification of the chemical elements while showing their spatial distribution. Although the mapping has not been acquired to quantify the elements, the signal intensity qualitatively reflects their local concentration. The mapping presented in Figure 5 suggests that the
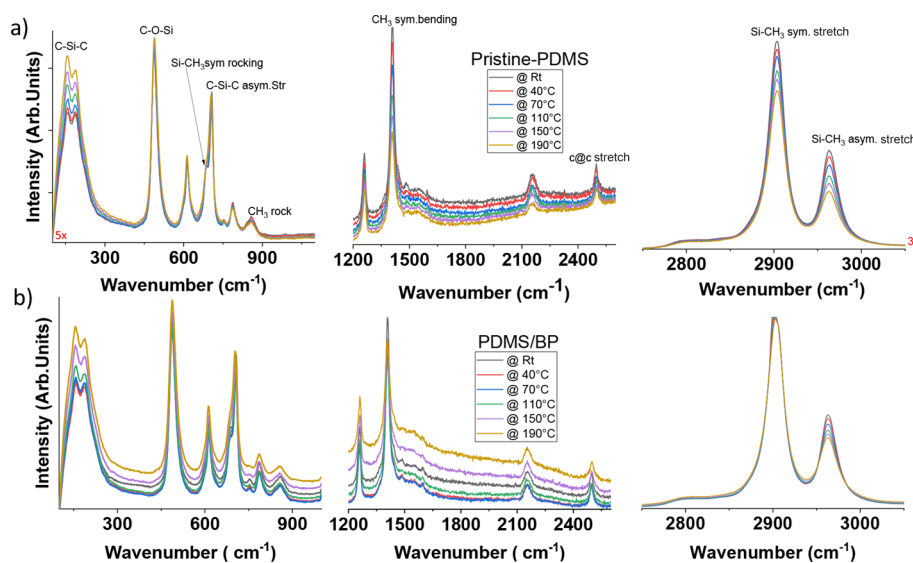
Figure 7. (a) Raman spectroscopy of Sylgard-PDMS pristine sample writing grating parameters (repetition rate 606 kHz, 8 passes, and 25 mm·s^{-1}) at different temperatures in three regions. (b) Raman spectroscopy of PDMS blended with the BP sample with parameters: repetition rate 606 kHz, two passes, and 5 mm·s^{-1} at different temperatures in three regions.

composition of the waveguides differs slightly from the matrix one. Carbon and oxygen signals are more intense at the region of the waveguide's cross-section, suggesting that this region presents a higher concentration of these atoms. Indeed, an EDS profile extracted from a line crossing multiple laser inscriptions demonstrates that they present a higher carbon and oxygen content and are slightly deficient in silicon than the PDMS matrix (Figure 5, bottom left). The germanium content appears to be unaffected by the laser inscription; however, the low concentration of the Ge atoms in the composite approaches the detection limit in EDS. Thus, from these data, it is unclear whether the germanium concentration is locally affected by the laser inscription.

The waveguides were imaged by AFM (Figure 6), where both topographical and phase images were recorded for PDMS/BP + Ge. The waveguide relief created during the cryo-fracture is approximately 300 nm in relation to the surrounding PDMS surface, and the grainy structure observed in SEM images is also present in topographical images. Therefore, the origin of the small particles present within the waveguide is the sample itself rather than some imaging artifact. Figure 6c depicts a higher magnification of the central section of a waveguide. Particles of ca. 30−40 nm are ubiquitous inside the zone affected by the laser inscription. The phase images (Figure 6b,d) suggest that the waveguides present a stiffer mechanical response than the PDMS matrix, corroborating the results presented in Section 2.9 "Tensile Test". Rather than the particles, the phase image suggests that the major source of a mechanical phase shift, i.e., a local increase in the stiffness is the medium surrounding them.

2.8. Variable-Temperature Raman (VT-Raman). The chemical compositions of *fs*-laser writing on PDMS elastomeric composites were investigated by Raman spectroscopy to probe the structural changes upon heating. Owing to the photo-sensitivity and the generation of radicals, all samples had a high fluorescence background; therefore, the relative intensities between the different spectra of the same samples were calculated. A typical Raman spectrum presented in Figure 7a shows the following vibrational modes of the pristine PDMS elastomer material for Si−, C−, O$_2$, and H$_2$ bonds; these include specific characteristics of various chemical stretches such as 488 cm^{-1} (Si−O−Si$_{(sym\ stretching)}$); 685 cm^{-1} (Si−CH$_{3(sym\ rocking)}$); 707 cm^{-1} (Si−C$_{(sym\ stretching)}$); 787 cm^{-1} (CH$_{3(asym\ rocking)}$ and Si−C$_{(asym\ stretching)}$); 858 cm^{-1} (CH$_{3(sym\ rocking)}$); 1262 cm^{-1} (CH$_{3(sym\ bending)}$); 1411 cm^{-1} (CH$_{3(asym\ bending)}$); 2909 cm^{-1} (CH$_{3(sym\ stretching)}$); and 2970 cm^{-1} (CH$_{3(asym\ stretching)}$). These assignments are in good agreement with those found in the literature.[34] The Raman and IR spectra of the selected composites are shown in the SI.

Next, we studied the effect of temperature on the grating PDMS samples, mainly in selected three spectroscopic regions for clarity. The intensity of the bands was mostly attributed to C−Si−C, Si−O−Si, and Si−C$_{(sym)}$ bonds in the PDMS control. Note that the intensity of these stretches increases with the increase in temperature. In contrast, the intensity of the CH$_{3(sym\ rocking)}$ in the following peaks 685, 707, 858, and 787 cm^{-1} was decreasing, and it can be related to the breaking of the Si−CH$_3$, Si−C, and CH$_3$ bonds. The shoulder at 685 cm^{-1} assigned to Si−CH$_{3(sym\ rocking)}$ disappears after heating to 70 °C; this can be related to the formation of the microcrystalline Si−C bonds. Another decrease in the intensity was observed in the second and the third selected regions from 1200−2600, 2800−3000 cm^{-1} assigned for CH$_{3(sym\ bending)}$ and Si−CH$_{3(sym\ and\ asym\ stretches)}$, respectively, as the temperature increased. To summarize, the temperature has a direct effect on the rocking stretches and leads to a weak decrease in the intensity as bonds are breaking, whereas the other stretches exhibit a slight increase in the intensity owing to the formation of new bonds. The resulting details of all described samples and their assignments of the bands and intensities are given in the SI.

For comparison, we have selected the PDMS/BP blend, as shown in Figure 7b. All the selected organic and inorganic photoinitiator-based PDMS materials are organized in the SI. The results indicate an increase in the regions attributed to the C−Si−C, Si−O−Si, and Si−C$_{(sym)}$ bands in the PDMS and a decrease in the intensity of the Si−CH$_{3(asym\ rocking)}$ as expected. Interestingly, the Si−CH$_{3(sym)}$ at 2900 cm^{-1} exhibits no change in intensity, and we hypothesized that the BP is reacting with vinyl bonds rather than the CH$_3$-functionalities during the

radical reaction. Similar behavior to that of the BP composite was observed in the case of IGR-184. However, switching to PDMS/Ge, the same Si−CH$_{3(sym rocking)}$ stretch did not show any changes because the Ge complex has a C−CH$_3$ symmetric deformation, and this also appeals to the composite of PDMS/ Ge + BP. It is worth mentioning that the Ge and Ge + BP-based composites led to the formation of three new peaks that were not assigned and require further investigation. In general, we observed from Raman spectra that *fs*-laser writing causes major deformation in the PDMS structure in all composites.

2.9. Tensile Test. The mechanical experiments were performed on PDMS-Sylgard as a controller, and some selected composites (PDMS/Ge, PDMS/BP-Ge, and PDMS/ IRG 184) before and after writing/grating were tested. The experiments were performed in triplicates. Here, we report the engineering stress, strain, and Young's modulus as average values and their corresponding standard deviations. The samples before writing showed a lower Young's modulus with improved elongation at the break event displaying a classical trend. Note that the chain extenders or the reactive photoinitiators that react with both PDMS would create a grafted composite, enhancing the elongation (Table 2). The

Table 2. Tensile Strength Values (MPa), Young's Modulus Values (GPa), and Elongation at Break (%) of PDMS Compositions before Writing and after fs-Laser Writing

composites	tensile strength [MPa]	Young's modulus [GPa]	elongation at break [%]
PDMS compositions before fs-laser writing			
PDMS/controller	2.1 ± 0.6	6.51 ± 1.61	76 ± 2.3
PDMS/BP	0.6 ± 0.08	1.19 ± 0.03	66 ± 9.4
PDMS/ATEG	0.42 ± 0.2	0.8 ± 0.17	60 ± 21.4
PDMS/IRG 184	1.8 ± 1.3	3.7 ± 1.52	65 ± 17.4
PDMS/BP + Ge	0.91 ± 12	1.67 ± 0.56	107 ± 13.62
PDMS compositions after fs-laser writing			
PDMS/controller	3.65 ± 1.4	9.34 ± 1.77	90 ± 25.29
PDMS/ATEG	0.1 ± 0.06	0.79 ± 1.17	22 ± 10.08
PDMS/IGR 184	0.74 ± 0.4	2.19 ± 0.04	62 ± 19.33
PDMS/BP + Ge	0.42 ± 1.56	3.08 ± 1.0	92 ± 19.86

Young's modulus displayed after writing was as expected for PDMS/Ge and PDMS/IRG 184 led to the *sacrifice of the mechanical properties* in tensile strength. The tensile strength results are reported in Table 2. Note that a high elongation represents an improvement in the impact property of the material; otherwise, it shows brittleness.

2.10. Dynamical Study vs Temperature. The dynamic study was performed in parallel with variable-temperature Raman spectroscopy to observe any changes that may occur in the structural and mechanical properties. In this study, we kept a constant frequency of 1 Hz, in which storage and loss modulus were calculated by TA Average Instruments (Figure S10 and Table S9). The selected samples were measured over the temperature range of 40−190 °C and at temperature increments of 30 °C. All the samples behave similarly, but the PDMS/BP composite shows a fluctuation in storage and loss modulus with an increase in temperature of 100 °C. The reason behind these fluctuations is the BP photoinitiator's slow radical formation and chemical reactivity.[35] The chemical reactivity of the BP was observed to stabilize above 100 °C, as shown in the SI.

2.11. Kinetic Study of the Aging Process. To understand the effect of aging on the studied materials after fs-laser writing, we performed a kinetic study. Our aging measurements were dependent on several writing parameters reported previously by us,[28] such as a power range from 4 to 8 mW, a writing speed of 20 mm·s^{-1}, a repetition rate in the range of 101−606 kHz, $\lambda_{writing}$ of 515 nm, a pulse width of 250 fs, number of passes 1−8, and focus lens (NA) of 0.01 and 0.25. These parameters can vary between photoinitiators depending on their chemical sensitivity.

The pristine PDMS and selected samples were analyzed for RI change at two different times: T_0 (starting testing time) and T_f (final testing time). In the case of the control, the main observations were that there are no significant changes over aging time and RI change, remain intact, and transparent. Moreover, similar observations in comparison to the controller were found in the blends of PDMS with BP, Ge, and IRG 184 at both repetition rates (101 and 606 kHz, see the SI). In contrast, the PDMS/BP + Ge composite exhibits lower tolerability when the sample was aged at a high repetition rate of 606 kHz (Figure 8).

In addition to the aging time, we conducted thermal aging as an example of the PDMS/IRG 184 composite (Figures S19 and S20). Noteworthy, all the PDMS composites were thermally exposed after fs-laser writing in order to verify their thermal resilience. We placed the samples at a given temperature for nearly 1 h in the oven, followed by slow cooling under ambient conditions. Only then the measurements were conducted in triplicates at each temperature. The sample was tested at a temperature range between 40 °C and 190 °C involving two repetition rates (606 and 101 kHz). The sample at the repetition rate of 101 kHz had a lower RI change above 150 °C. In contrast, replacing the repetition rate with 606 kHz resulted in an even lower RI change above 130 °C. This is expected owing to the use of higher power combined with heat accumulation. Notably, both repetition rates have an optimal RI change at 70 °C. We hypothesized that at this specific temperature, we obtained the highest amorphization degree that increases the flexibility of the polymer chains, thus increasing the RI change, whereas at a higher temperature of 70 °C, the polymer begins to burn. Finally, we decided to study the effect of three selected solvents on the writing shape and morphology. The studied samples PDMS/BP + Ge and PDMS/BP were soaked in acetone, isopropanol, and water for periods of 1 and 24 h. Images of the samples before soaking, when the samples were wet, and after drying were obtained using a digital microscope. Water had minimal to no effect on the shape or morphology of the samples. In contrast, both acetone and isopropanol result in swelling of the samples (images are shown in Figure S21).

3. CONCLUSIONS

In conclusion, this study represents a significant contribution to the ongoing exploration of photosensitized PDMS and its potential application for fs-laser writing. By investigating the effects of fs-laser writing on the polymer structure, mechanical properties, and optical characteristics, we have gained valuable insights into the behavior and performance of PDMS under different conditions. We demonstrated a significant advancement in the refractive index change, achieving a remarkable 15-fold improvement in the case of PDMS/BP-Ge (a composite of benzophenone (BP) and allytriethylgermane). Furthermore, the optical performance levels of the PDMS composites,
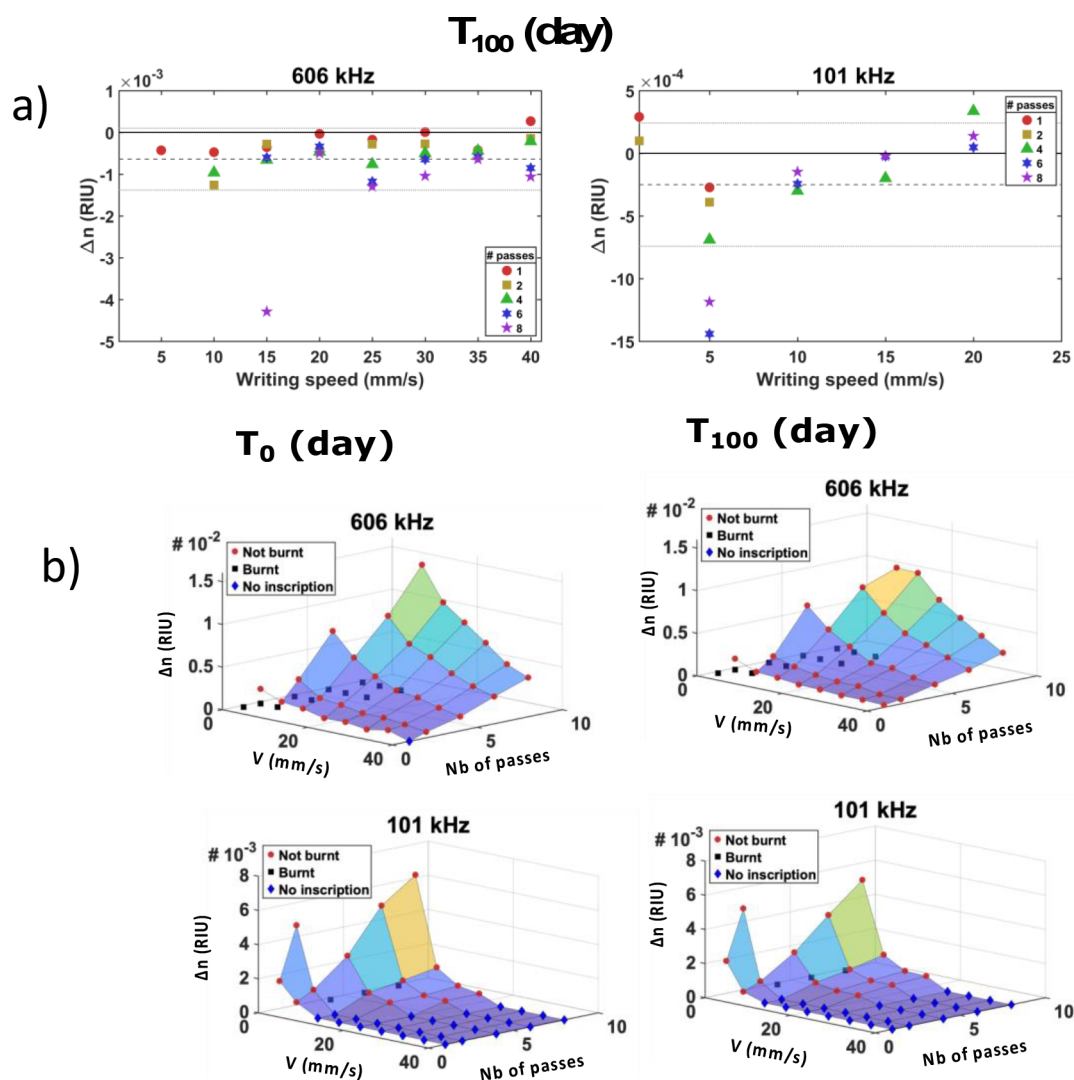
Figure 8. Modulation vs writing speed of PDMS/BP + Ge at T_f = 100 days, at two different repetition rates of 606 and 101 kHz based on (a) 2D and (b) 3D presentations combined with the refractive index change (RIU), the velocity of the writing of *fs* waveguide, and the number of passes.

including Irgacure 184/500, BP-Ge, and Ge-ATEG, show a relative difference of less than 5% when compared to pristine PDMS, placing them on par with glass materials. Also, the polymer composites (e.g., PDMS/IRG 184 composite) were stable and transparent over the aging time, with no significant changes in RI change. The fs-induced RI change varied with the repetition rate, showing a lower RI change at an aging temperature above 150 °C for 101 kHz and an even lower RI change above 130 °C for 606 kHz due to higher power and heat accumulation.

These findings highlight the potential of specific photoinitiators, such as BP-Ge, to greatly enhance the refractive index change and optical properties of PDMS. One of the key aspects of our research was the careful selection of organic and inorganic photoinitiators, which played a crucial role in generating radical initiations within the polymer backbone. The fundamental characteristics of PDMS and its response to temperature variations, refractive index changes, and aging were thoroughly investigated. The outcome of these observations shows that the selection of a photoinitiator is crucial and can be adjusted according to the desired chemical, mechanical, and photonic properties of PDMS but is also significant as parameters of fs-laser writing.

4. MATERIALS AND METHODS

Composites were prepared according to our previously reported fabrication method.[28] Typically, the PDMS prepolymer containing divinyl-end groups (Sylgard-184: base material) was mixed at a high speed with 2−4% (w/w) of a photosensitizing agent and subsequently ultrasonicated for 15 min. To blend, a curing agent, containing Si−H functional groups, and a platinum catalyst were added in a ratio of 10:1 (w/w), and the mixture was sonicated for a further 1−2 min.

The blend was kept under a vacuum for 30 min to remove the air bubbles produced during the mixing process. The bubble-free liquid PDMS composites were then poured into a designed mold of 5 × 2 cm² with a depth of 1 mm, which was finally placed in an oven at 80 °C for 2 h. The set molds were removed, and the flexible films were allowed to cool to room temperature. The transparency of the films was observed visually and further studied by UV−vis spectroscopy before performing any laser-based writing, as shown in Figure 9. Samples were rejected if they showed the presence of aggregation, crystallization, or any signs of degraded mechanical quality.
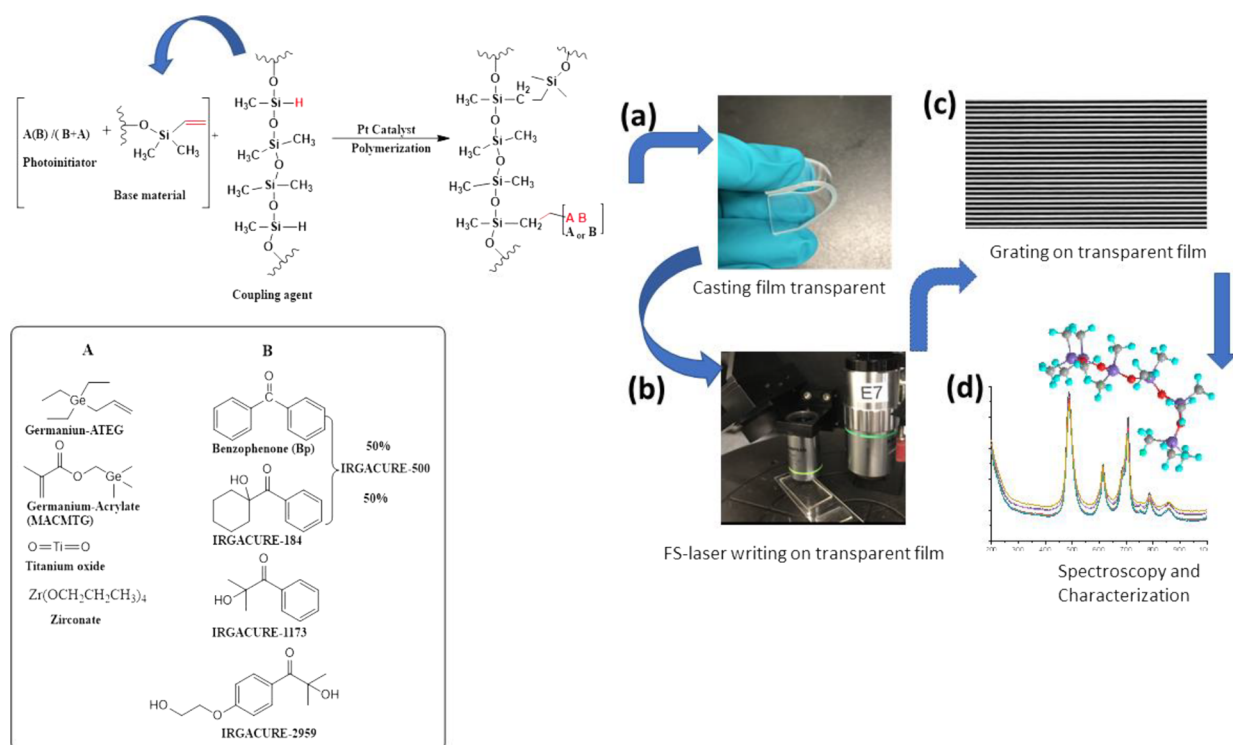
Figure 9. Schematic route for the fabrication of photosynthesized PDMS composites of the various [A (organometallics) and B (organics)] photoinitiators incorporated in PDMS. (a) Transparent film, (b) fs-laser writing scheme, (c) written sample side by side, and (d) analysis figure.

4.1. Femtosecond Writing.

Based on our previous data,[27,28] we wrote our inscription using a 250 fs laser at a wavelength of 515 nm, thus yielding a multiphoton absorption process in order to cross the bandgap. The repetition rate of the laser was changed from 101 to 606 kHz using a pulse picker to ensure that the pulse energy is conserved, and the intensity of the laser is 6.8×10^{12} W/cm^2,[36] while the writing speed was varied from 1 to 40 mm/s. The number of passes used to induce the RI change was changed from 1 to 8. The parameters were employed on every sample to map the RI change. The pulse energy was kept constant at 6.6 nJ and was measured using an Olympus microscope lens with a numerical aperture (NA) of 0.4.

■ ASSOCIATED CONTENT

Ⓢ Supporting Information

The Supporting Information is available free of charge at https://pubs.acs.org/doi/10.1021/acsomega.3c01202.

> Description and results of UV−vis, PXRD, TGA, DSC, tensile stress, Raman, refractive index change, SEM, and AFM for selected compounds (PDF)

■ AUTHOR INFORMATION

Corresponding Author

Antsar R. Hlil − *Centre d'optique, Photonique et Laser, Université Laval, Québec, QC G1V 0A6, Canada; Fabulas Laboratory, Department of Electrical Engineering, École Polytechnique Montréal, Montreal, QC H3T 1J4, Canada; Département de chimie, Faculté des sciences et de génie Pavillon Alexandre-Vachon, Université Laval, Québec, QC G1V 0A6, Canada;* ⓞ orcid.org/0000-0002-1673-1268; Email: antsar.hlil@polymtl.ca

Authors

Jean-Sebastien Boisvert − *Fabulas Laboratory, Department of Physics Engineering, École Polytechnique Montréal, Montreal, QC H3T 1J4, Canada*

Hatem M. Titi − *Department of Chemistry, McGill University, Montréal, QC H3A 0G4, Canada;* ⓞ orcid.org/0000-0002-0654-1292

Yalina Garcia-Puente − *Fabulas Laboratory, Department of Physics Engineering, École Polytechnique Montréal, Montreal, QC H3T 1J4, Canada;* ⓞ orcid.org/0000-0003-4636-7150

Wagner Correr − *Centre d'optique, Photonique et Laser, Université Laval, Québec, QC G1V 0A6, Canada*

Sebastien Loranger − *Centre d'optique, Photonique et Laser, Université Laval, Québec, QC G1V 0A6, Canada; Fabulas Laboratory, Department of Physics Engineering, École Polytechnique Montréal, Montreal, QC H3T 1J4, Canada*

Jyothis Thomas − *Fabulas Laboratory, Department of Physics Engineering, École Polytechnique Montréal, Montreal, QC H3T 1J4, Canada*

Ali Riaz − *Centre d'optique, Photonique et Laser, Université Laval, Québec, QC G1V 0A6, Canada*

Younès Messaddeq − *Centre d'optique, Photonique et Laser, Université Laval, Québec, QC G1V 0A6, Canada; Département de chimie, Faculté des sciences et de génie Pavillon Alexandre-Vachon, Université Laval, Québec, QC G1V 0A6, Canada;* ⓞ orcid.org/0000-0002-0868-2726

Raman Kashyap − *Centre d'optique, Photonique et Laser, Université Laval, Québec, QC G1V 0A6, Canada; Fabulas Laboratory, Department of Electrical Engineering and Fabulas Laboratory, Department of Physics Engineering, École Polytechnique Montréal, Montreal, QC H3T 1J4, Canada*

Complete contact information is available at:
https://pubs.acs.org/10.1021/acsomega.3c01202

Author Contributions

A.H.: carried out the writing original draft/editing of the manuscript, design of experiments, performed all the experimental work as well as data curation and analysis and conceptualization. J.-S.B.: RI change analysis, fs-laser writing, and analysis. H.M.T.: measurement and analysis of PXRD, writing, review, and editing. Y.G.P.: visualization and review. S.L.: review and editing. J.T.: review and editing. A.R.: review and editing. W.C.: measurement and SEM and AFM analyses. Y.M.: supervision, resources, review, and editing. R.K.: conceptualization, resources, supervision, review, and editing.

Notes

The authors declare no competing financial interest.

■ REFERENCES

(1) Sugioka, K.; Cheng, Y. Ultrafast Lasers—Reliable Tools for Advanced Materials Processing. *Light Sci. Appl.* **2014**, *3*, No. e149.

(2) Gattass, R. R.; Mazur, E. Femtosecond Laser Micromachining in Transparent Materials. *Nat. Photonics* **2008**, *2*, 219−225.

(3) Sun, C.-K.; Vallée, F.; Acioli, L. H.; Ippen, E. P.; Fujimoto, J. G. Femtosecond-Tunable Measurement of Electron Thermalization in Gold. *Phys. Rev. B: Condens. Matter* **1994**, *50*, 15337−15348.

(4) Fann, W. S.; Storz, R.; Tom, H. W.; Bokor, J. Electron Thermalization in Gold. *Phys. Rev. B: Condens. Matter* **1992**, *46*, 13592−13595.

(5) Nolte, S.; Kamlage, G.; Korte, F.; Bauer, T.; Wagner, T.; Ostendorf, A.; Fallnich, C.; Welling, H. Microstructuring with Femtosecond Lasers. *Adv. Eng. Mater.* **2000**, *2*, 23−27.

(6) Loesel, F. H.; Fischer, J. P.; Götz, M. H.; Horvath, C.; Juhasz, T.; Noack, F.; Suhm, N.; Bille, J. F. Non-thermal Ablation of Neural Tissue with Femtosecond Laser Pulses. *Appl. Phys. B: Lasers Opt.* **1998**, *66*, 121−128.

(7) Chkalov, R.; Chkalova, D. Femtosecond Laser Micromachining Complex Based on a Telecommunication Network. *AIP Conf. Proc.* **2022**, *2647*, No. 040016.

(8) Zhang, Y.-L.; Chen, Q.-D.; Xia, H.; Sun, H.-B. Designable 3D Nanofabrication by Femtosecond Laser Direct Writing. *Nano Today* **2010**, *5*, 435−448.

(9) Ams, M.; Marshall, G. D.; Dekker, P.; Piper, J. A.; Withford, M. J. Ultrafast Laser Written Active Devices. *Laser Photon. Rev.* **2009**, *3*, 535−544.

(10) Khorasani, M. T.; Mirzadeh, H.; Sammes, P. G. Laser Induced Surface Modification of Polydimethylsiloxane as a Super-Hydrophobic Material. *Radiat. Phys. Chem.* **1996**, *47*, 881−888.

(11) Mikutis, M.; Kudrius, T.; Šlekys, G.; Paipulas, D.; Juodkazis, S. High 90% Efficiency Bragg Gratings Formed in Fused Silica by Femtosecond Gauss-Bessel Laser Beams. *Opt. Mater. Express* **2013**, *3*, 1862.

(12) Jung-Kyu, P.; Sung-Hak, C.; Kwang-Ho, K.; Myung-Chang, K. Optical Diffraction Gratings Embedded in BK-7 Glass by Low-Density Plasma Formation Using Femtosecond Laser. *Trans. Nonferrous Met. Soc. China* **2011**, *21*, s165−s169.

(13) Du, D.; Liu, X.; Korn, G.; Squier, J.; Mourou, G. Laser-Induced Breakdown by Impact Ionization in SiO_2 with Pulse Widths from 7 Ns to 150 Fs. *Appl. Phys. Lett.* **1994**, *64*, 3071−3073.

(14) Boisvert, J.-S.; Hlil, A.; Thomas, J.; Garcia-Puente, Y.; Riaz, A.; Ledemi, Y.; Messaddeq, Y.; Kashyap, R. Photosensitivity Functionalization of PDMS for Femtosecond Laser Writing. In *Novel Optical Materials and Applications*; Optical Society of America, 2020, NoTh1C.

(15) Panusa, G.; Pu, Y.; Wang, J.; Moser, C.; Psaltis, D. Multiphoton Fabrication of Ultra-compact Optical Waveguides in Polydimethylsiloxane. In *International Conference on Optical M.E.M.S. and Nanophotonics (OMN)*; IEEE Publications, 2018; Vol. *2018*, pp. 1−5.

(16) Deepak, K. L. N.; Soma, V. R.; Desai, N. R. *Direct Writing in Polymers with Femtosecond Laser Pulses: Physics and Applications*, Peshko, I., Ed.; InTech Publishers, 2012; pp. 277−294.

(17) Terakawa, M. Femtosecond Laser Processing of Biodegradable Polymers. *Appl. Sci.* **2018**, *8*, 1123.

(18) Duffy, D. C.; McDonald, J. C.; Schueller, O. J.; Whitesides, G. M. Rapid Prototyping of Microfluidic Systems in Poly-(Dimethylsiloxane). *Anal. Chem.* **1998**, *70*, 4974−4984.

(19) Wolfe, D. B.; Ashcom, J. B.; Hwang, J. C.; Schaffer, C. B.; Mazur, E.; Whitesides, G. M. Customization of Poly-(Dimethylsiloxane) Stamps by Micromachining Using a Femtosecond-Pulsed Laser. *Adv. Mater.* **2003**, *15*, 62−65.

(20) Potter, B. G., Jr.; Simmons-Potter, K.; Chandra, H.; Jamison, G. M.; Thomes, W. J., Jr. Photoprogrammable Molecular Hybrid Materials for Write-as-Needed Optical Devices. *J. Non-Crystal. Solids* **2006**, *352*, 2618−2627.

(21) Hasegawa, T.; Oishi, K.; Maruo, S. Three-Dimensional Microstructuring of PDMS by Two-Photon Microstereolithography. In *IEEE. International Symposium on Micronano Mechanical and Human Science*; IEEE Publications, 2006; Vol. *2006*, pp. 1−4.

(22) Coenjarts, C. A.; Ober, C. K. Two-Photon Three-Dimensional Microfabrication of Poly(Dimethylsiloxane) Elastomers. *Chem. Mater.* **2004**, *16*, 5556−5558.

(23) Selvaraj, H.; Tan, B.; Venkatakrishnan, K. Maskless Direct Micro-structuring of PDMS by Femtosecond Laser Localized Rapid Curing. *J. Micromech. Microeng.* **2011**, *21*, No. 075018.

(24) Hlil, A.; Boisvert, J. S.; Lorre, P.; Iden, H.; García-Puente, Y.; Ledemi, Y.; Messaddeq, Y.; Kashyap, R. Nofphem: Novel Optical Fibres and Photosensitive Elastomeric Materials. In *21st International Symposium on Non-Oxide and New Optical Glasses* 2018; Vol. *24*, June 21.

(25) Panusa, G.; Pu, Y.; Wang, J.; Moser, C.; Psaltis, D. Photoinitiator-Free Multi-photon Fabrication of Compact Optical Waveguides in Polydimethylsiloxane. *Opt. Mater. Express* **2019**, *9*, 128.

(26) Graubner, V.-M.; Nuyken, O.; Lippert, T.; Wokaun, A.; Lazare, S.; Servant, L. Local Chemical Transformations in Poly-(Dimethylsiloxane) by Irradiation with 248 and 266nm. *Appl. Surf. Sci.* **2006**, *252*, 4781−4785.

(27) Boisvert, J.-S.; Thomas, J.; Lorre, P.; Hassan, I.; Ledemi, Y.; Messaddeq, Y.; Kashyap, R. Novel Functionalization of PDMS for Photosensitivity. *Integr. Opt. Devices Mater. Technol.* **2019**, *XXIII*.

(28) Boisvert, J. S.; Hlil, A.; Loranger, S.; Riaz, A.; Ledemi, Y.; Messaddeq, Y.; Kashyap, R. Photosensitization Agents for Fs Laser Writing in PDMS. *Sci. Rep.* **2022**, *12*, 1623.

(29) Tan, D.; Sharafudeen, K. N.; Yue, Y.; Qiu, J. Femtosecond Laser Induced Phenomena in Transparent Solid Materials: Fundamentals and Applications. *Prog. Mater. Sci.* **2016**, *76*, 154−228.

(30) Žukauskas, A.; Batavičiūtė, G.; Ščiuka, M.; Jukna, T.; Melninkaitis, A.; Malinauskas, M. Characterization of Photopolymers Used in Laser 3D Micro/Nanolithography by Means of Laser-Induced Damage Threshold (LIDT). *Opt. Mater. Express* **2014**, *4*, 1601.

(31) Adams, A. C.; Schinke, D. P.; Capio, C. D. An Evaluation of the Prism Coupler for Measuring the Thickness and Refractive Index of Dielectric Films on Silicon Substrates. *J. Electrochem. Soc.* **1979**, *126*, 1539−1543.

(32) Metricon Corporation. http://www.metricon.com.

(33) Camino, G.; Lomakin, S. M.; Lazzari, M. Polydimethylsiloxane Thermal Degradation Part 1. Kinetic Aspects. *Polymer* **2001**, *42*, 2395−2402.

(34) Bae, S. C.; Lee, H.; Lin, Z.; Granick, S. Chemical Imaging in a Surface Forces Apparatus: Confocal Raman Spectroscopy of Confined Poly(Dimethylsiloxane). *Langmuir* **2005**, *21*, 5685−5688.

(35) Carbone, N. D.; Ene, M.; Lancaster, J. R.; Koberstein, J. T. Kinetics and Mechanisms of Radical-Based Branching/Cross-Linking

Reactions in Preformed Polymers Induced by Benzophenone and Bis-Benzophenone Photoinitiators. *Macromolecules* **2013**, *46*, 5434−5444.

(36) Skliutas, E.; Lebedevaite, M.; Kabouraki, E.; Baldacchini, T.; Ostrauskaite, J.; Vamvakaki, M.; Farsari, M.; Juodkazis, S.; Malinauskas, M. Polymerization mechanisms initiated by spatio-temporally confined light. *NANO* **2021**, *10*, 1211−1242.